Acta Geologica Polonica, Vol. 66 (2016), No. 3, pp. 473–491
DOI: 10.1515/agp-2016-0021

Hydrothermal metasomatism of a peralkaline granite pegmatite, Khaldzan Buragtag massif, Mongolian Altai; complex evolution of REE-Nb minerals

BOGUSŁAW BAGIŃSKI[1], PETRAS JOKUBAUSKAS[1], JUSTYNA DOMAŃSKA-SIUDA[1], PAVEL KARTASHOV[2] and RAY MACDONALD[1,3]

[1]*Institute of Geochemistry, Mineralogy and Petrology, Faculty of Geology of the University of Warsaw, Al. Żwirki i Wigury, 93, PL-02-089 Warszawa, Poland. E-mail: B.Baginski1@uw.edu.pl*
[2]*Institute of Ore Deposits, Russian Academy of Sciences, Moscow 119107, Russia*
[3]*Environment Centre, Lancaster University, Lancaster LA1 4YQ, UK*

ABSTRACT:

Bagiński B., Jokubauskas P., Domańska-Siuda J., Kartashov P. and Macdonald, R. 2016 Hydrothermal metasomatism of a peralkaline granite pegmatite, Khaldzan Buragtag massif, Mongolian Altai; complex evolution of REE-Nb minerals. *Acta Geologica Polonica*, **66** (3), 473–491. Warszawa.

The low-temperature hydrothermal alteration of certain rare-metal minerals is recorded in a quartz-epidote metasomatite from the Tsakhirin Khuduk occurrence in the Khaldzan-Buragtag Nb-REE-Zr deposit, Mongolian Altai. A peralkaline granitic pegmatite was metasomatized by hydrothermal fluids released from associated intrusions, with the formation of, *inter alia*, chevkinite-(Ce), fergusonite-(Nd) and minerals of the epidote group. The textural pattern indicates recrystallization and coarsening of these phases. Later, low-temperature alteration by fluids resulted in the chevkinite-(Ce) being replaced by complex titanite-TiO_2-cerite-(Ce)-hingganite-hydroxylbastnäsite-(Ce) assemblages. Calcite formed late-stage veins and patches. The hydrous fluids were poor in F and CO_2 but had high Ca contents.

Key words: Khaldzan-Buragtag Nb-REE-Zr deposit; Hydrothermal alteration; Composition of fluids; Chevkinite group minerals; REE minerals.

INTRODUCTION

Recent studies of the hydrothermal alteration of the chevkinite group of minerals (CGM) have revealed a diversity of alteration products, dependent, *inter alia*, on the composition of the host rock, the composition of the hydrothermal fluids and the pressure and temperature at which the alteration proceeded (Jiang 2006; Vlach and Gualda 2007; Bagiński *et al.* 2015; Macdonald *et al.* 2015 a, b, 2016). The diversity has consequences for the mobilization or retention of rare-metals and the significance for the formation of rare-metal deposits. This report examines the nature of the lower temperature fluids which altered the REE-actinide-HFSE minerals in a quartz-epidote metasomatite of the Khaldzan Buragtag peralkaline massif in Mongolia. For this, as in an earlier study of the metasomatite (Macdonald *et al*. 2016), particular attention is paid to minerals of the chevkinite group (CGM). The CGM, with general formula $(REE,Ca)_4Fe^{2+}(Fe^{2+}, Fe^{3+},Ti,Al)_2 Ti_2(Si_2O_7)O_8$, are increasingly being recognised as important carriers of the REE (with up to 50 wt% REE_2O_3), HFSE and, in some cases, the actinides. They have the potential, therefore, to carry important

records of the mobility of these elements during the fluid-influenced post-magmatic stages of the deposit.Combining the results of this study and those of Macdonald *et al*. (2016), we comment on the changes in fluid composition as the fluids migrated away from the host massif.

GEOLOGICAL SETTING

The Haldzan Buragtag Nb-Zr-REE deposit is located in the Mongolian Altai, some 45 km northeast of the city of Kobdo (Text-fig. 1). It is related to two bodies of peralkaline granite which are part of the multiphase Haldzan Buragtag peralkaline massif which is exposed in two oval-shaped outcrops (northern and southern) about 1 km apart (Kovalenko *et al*. 1995; Andreev and Ripp 1996). The massif, which is 30 km long and up to 8 km wide, was intruded at ~385 Ma into Cambrian volcanic and sedimentary rocks and granites, and a series of dolerites and gabbros. It is partly covered by Devonian volcanic rocks.

In the Tsakhirin Khuduk occurrence at the northern end of the Haldzan Buragtag massif, quartz-epidote metasomatites form two types of body: linear zones

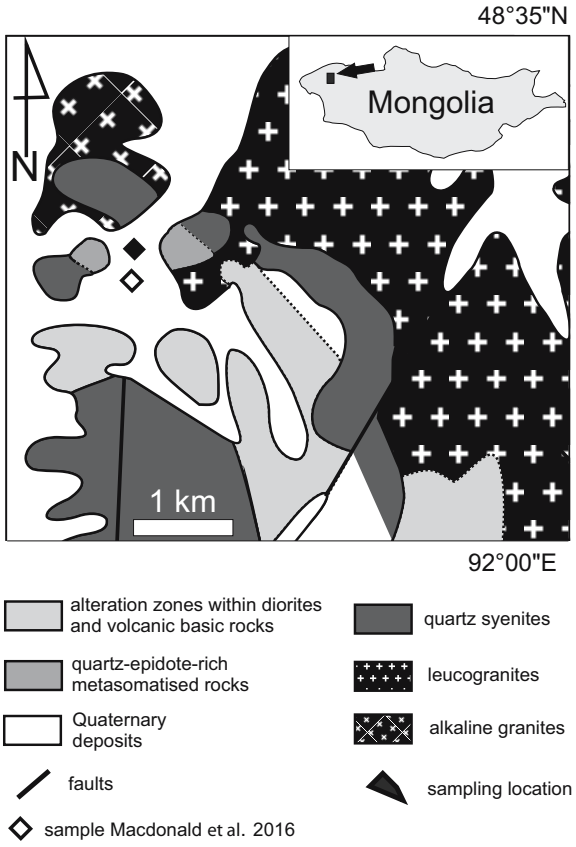

Text-fig. 1. Locality map of the Khaldzan Buragtag massif

0.5–20 m thick and up to 400 m long, and elliptical stockworks up to 150 × 200 m in size. Two linear zones (Western and Eastern) are more enriched in rare-metals than the stockwork bodies. The zones occur at the exocontact of the massif, here represented by quartz syenites of an early intrusive phase, with Cambrian volcanic rocks, granites and doleritic rocks. Field and petrographic evidence indicates that the linear zones are large, metasomatically altered, pegmatite bodies (or series of subparallel pegmatitic veins) derived from peralkaline granites not exposed at the current erosion level. The metasomatites inherited the structural features, mineralogy and rare-metal content of the pegmatites which they replaced. For example, different zones in the pegmatite can still be recognised, such as the outer part of the block zone through the inner part of the block zone to the quartz core. The host dolerites were, at the same time, replaced by actinolite-feldspar-epidote, actinolite-epidote, and epidote metasomatites.

With increasing distance from the main granite of the massif, the grade of the ore zone becomes lower and there is also an increase in the degree of metasomatic alteration. This study focusses on a sample from the Western ore zone between trenches #4 and #3. It is complementary to the study by Macdonald *et al*. (2016) of material nearer to the intrusive massif and thus richer in ores.

ANALYTICAL METHODS

Mineral compositions were determined by electron microprobe at the Inter-Institute Analytical Complex at the Institute of Geochemistry, Mineralogy and Petrology, University of Warsaw, using a Cameca SX-100 microprobe equipped with four wavelength dispersive spectrometers. The accelerating voltage was 15 kV and the probe current was 20 or 40 nA. Counting times were 20 s on peak and 10 s on each of two background positions. The standards, crystals and X-ray lines used and detection limits, for chevkinite as an example, are given in the Appendix. Analytical conditions for other minerals may be found in Bagiński *et al.* (2016). The 'PAP' φ(ρZ) program (Pouchou and Pichoir 1991) was used for corrections. Back scattered electron (BSE) images were made on the same equipment as the mineral analyses. Representative analyses are presented in Tables 1 to 6; the full data set is given in Supplementary Tables 1 and 2. Lacking structural information, it is unknown whether the ThSiO4 phase in the metasomatite is thorite or huttonite. For simplicity, it is here termed thorite.

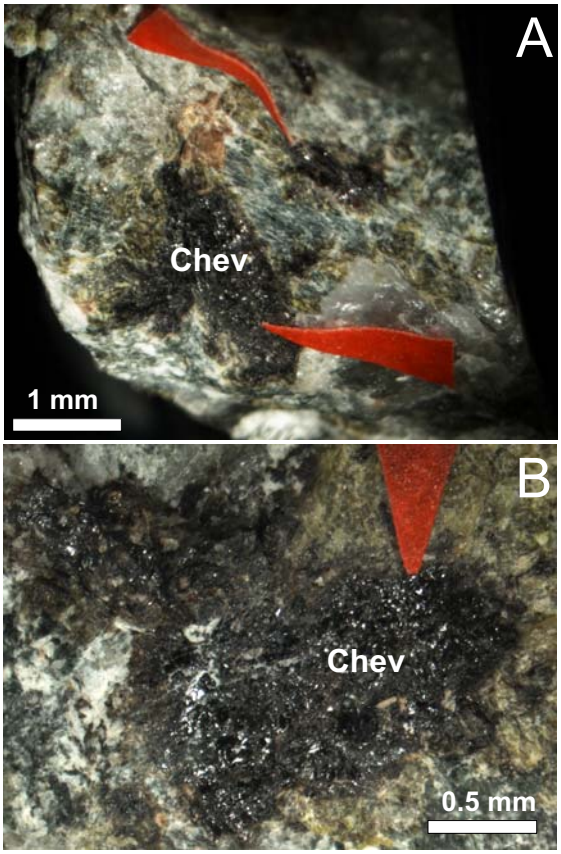

Text-fig. 2. (A) Photograph of chevkinite-(Ce) (red arrows) in matrix of quartz, epidote group minerals and hydroxylbastnäsite-(Ce). The white spots on chevkinite-(Ce) are reflections. (B) Detailed view of A

PETROGRAPHY

The mineralogy of the primary pegmatites can be deduced from other, less altered, pegmatites in the area, notably Tatyana (Kartashov *et al*. 1993), Neprimetnyi (Kartashov *et al*. 2002) and Geophysicheskii (Sokolova *et al*. 2004). They contained quartz, alkali feldspar, riebeckite-arfvedsonite and aegirine, with eudialyte, zircon, fergusonite-(Y), chevkinite-(Ce), hingganite-(Y) and epidote group minerals. The fergusonite, chevkinite and zircon form disseminated grains never exceeding 1 mm in size. The metasomatite consists mainly of quartz and epidote, with subordinate amounts of chevkinite, fergusonite, zircon and (ferri)allanite. The epidote formed by the breakdown of feldspar, arfvedsonite and aegirine in the pegmatite. The chevkinite, fergusonite and zircon crystals formed by recrystallization and enlargement of the same minerals in the primary pegmatite. The chevkinite in the metasomatite forms thin prismatic crystals

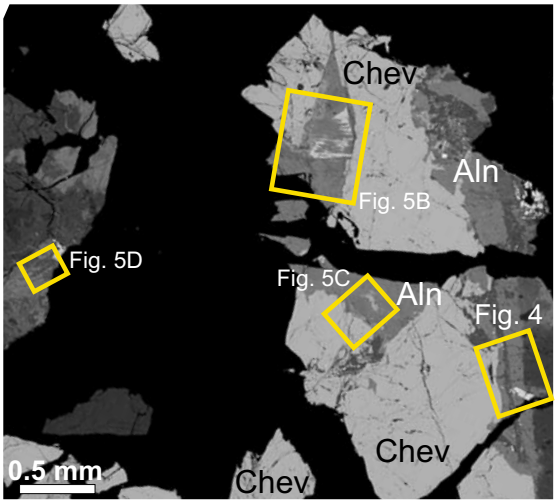

Text-fig. 3. Fragments of metasomatite showing the locations of Fig. 4 and Figs 5B, C, D. The location of Fig. 5A is shown on Fig. 4

2–3 × 0.3 cm in size (Text-fig. 2). Fluorite has not been recorded.

In detail, the sequence of crystallization events and the mineral products vary within the metasomatite at the selected site. The features described here represent the main events; the positions of the following images are shown on Text-fig. 3. The BSE image in Text-fig. 4 shows the chevkinite in contact with ferriallanite-(Ce). Mostly the contact is sharp but in the upper part of the image, the ferriallanite-(Ce) can be seen to have replaced the chevkinite-(Ce). To the bottom (in Text-fig. 4A), the ferriallanite-(Ce) is replaced by epidote, in turn

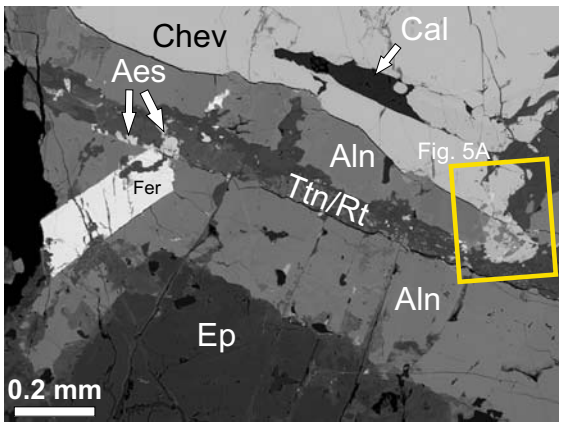

Text-fig. 4. Chevkinite-(Ce) (Chev) replaced along a sharp contact by ferriallanite-(Ce) (Aln); which is in turn replaced by epidote (Ep; dark grey) and by patches of an epidote of different composition (very dark grey). The ferriallanite-(Ce) is cut, in the centre of the image, by a vein of intergrown titanite (Ttn) and TiO_2 (Rt), which also forms veinlets and patches in the allanite. The vein includes some disseminated clusters of fergusonite (Fer). The large euhedral fergusonite-(Y) is considered to have been coeval with the growth of the chevkinite-(Ce). The position of Fig. 5A is shown

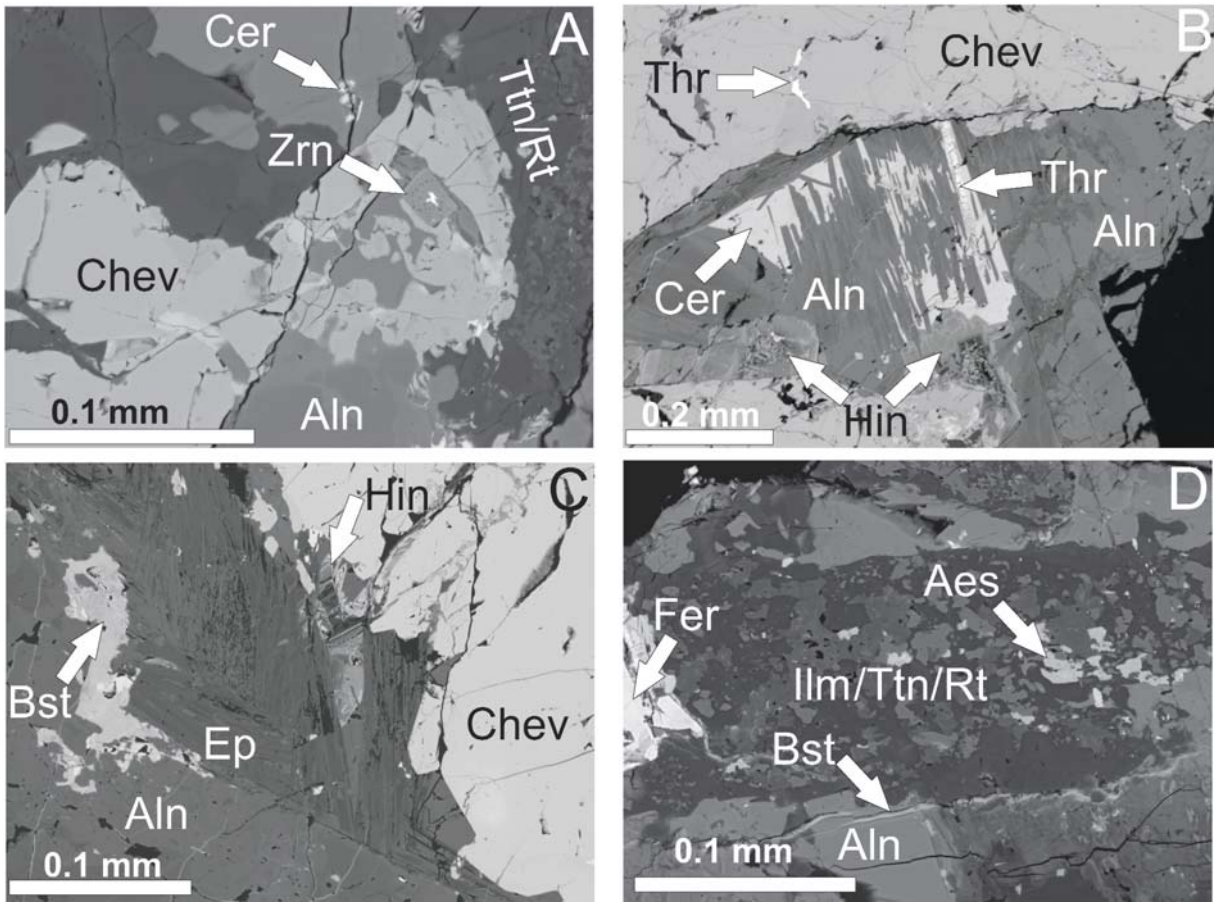

Text-fig. 5. **A** Magnification of part of Fig. 4. The light grey phase is chevkinite-(Ce), being partially replaced by patchily textured ferriallanite-(Ce) and then partly replaced by titanite and TiO_2. The anhedral bright grains in the chevkinite-(Ce) are cerite-(Ce) (Cer). The euhedral zircon (Zrn) crystal is taken to have been coeval with chevkinite crystallization. **(B)** Unaltered chevkinite-(Ce) in sharp contact with patchily zoned ferriallanite (darker and lighter). The comb-like phase is cerite-(Ce), containing a small string of thorite (Thr). An aggregate of hingganite grains (Hin) occurs along the chevkinite-ferriallanite boundary. **(C)** Chevkinite in irregular contact with a hair-like intergrowth of allanite-(Ce) (lighter) and epidote (darker), themselves replacing an earlier ferriallanite-(Ce). The L-shaped grain on the left is hydroxylbastnäsite-(Ce) (Bst). **(D)** Detail of the alteration of ferriallanite-(Ce) to titanite and rutile, in this case with ilmenite (Ilm). The bright grains in the titanite-rutile zone are mainly aeschynite-(Ce) (Aes)

patchily replaced by an epidote of different composition, which is rather darker on the BSE image. The main area of ferriallanite-(Ce) is cut by a veinlet of titanite (dark), a TiO_2 phase (dark grey), with dispersed grains of Nb,Y oxides (bright) and locally cerite-(Ce) (not seen on this image). The veinlet penetrates the ferriallanite-(Ce) in the centre of the image and directly replaces chevkinite-(Ce) at centre-right (Text-fig. 4). The large euhedral crystal of fergusonite-(Y) is cut by veinlets of both titanite and allanite and, like the small euhedral zircon in Text-fig. 5A, is probably a primary phase coeval with chevkinite crystallization. The elongated dark area in the chevkinite-(Ce) is calcite; it is taken to be a late-stage phase because calcite veins cut all zones in other parts of the metasomatite.

In Text-fig. 5B, chevkinite-(Ce) containing a small anhedral grain of thorite is in sharp contact with ferriallanite-(Ce) which is being replaced in patches and along strips by epidote. The medium-grey material is cerite-(Ce) and it appears to have intergrown with the epidote group minerals during alteration. The darker grey anhedral phase, partially replacing the cerite and allanite, is Nd-dominant hingganite. There is some variation in intensity from brighter to darker, the darker apparently replacing the lighter. Thorite forms the string of bright phases in the cerite. Text-fig. 5C shows a hair-like intergrowth of two varieties of epidote and residual patches of ferriallanite-(Ce). The L-shaped grain is hydroxylbastnäsite-(Ce), with an inclusion of cerite. Cerite also occurs as thin veinlets.

The replacement of ferriallanite-(Ce) by titanite and TiO_2 was in places complemented by the addition of ilmenite (Text-fig. 5D). The larger anhedral grain at left is fergusonite-(Y) and the rounded grain at right-central

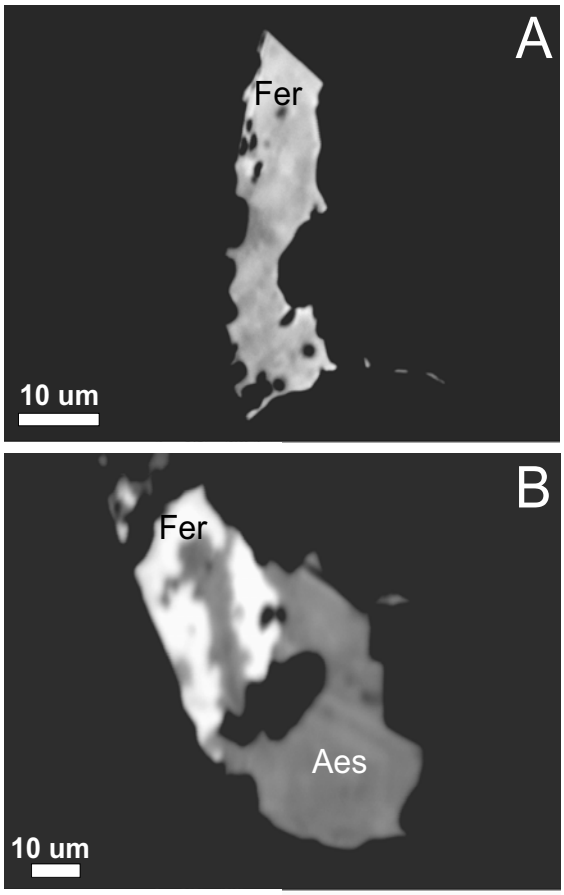

Text-fig. 6. **(A)** Heavily resorbed, patchy fergusonite-(Nd) at the contact between allanite and titanite-TiO_2 zones. **(B)** Bright fergusonite-(Nd) being replaced by dark grey aeschynite-(Y), also at the contact between ferriallanite and titanite-TiO_2 zones

is aeschynite-(Ce). The other bright grains are mainly aeschynite. The thin veins are cerite and REE-carbonate. Text-fig. 6 demonstrates two forms of fergusonite, both occurring at the boundary between the allanite and titanite-TiO_2 zones and both taken to be of early crystallization. The corroded, patchily zoned prism in Text-fig. 6A is fergusonite-(Nd) (brighter) zoned to fergusonite-(Ce) (darker); the stubby prism in Text-fig. 6B shows fergusonite-(Nd) (brighter) being replaced by darker grey aeschynite-(Y).

Sequence of events

The textural evidence is interpreted to show the following sequence of events. It should be stressed that the sequence is seen as essentially continuous, as the mineral assemblages changed in response to changing fluid composition and temperature decrease.

Formation of chevkinite-(Ce), fergusonite-(Y) and zircon (Text-figs 4, 5)
↓
Formation of ferriallanite-(Ce), partially replacing chevkinite (Text-fig. 4)
↓
Partial replacement of ferriallanite-(Ce) by epidote (Text-figs 4, 5)
↓
Formation of titanite and TiO_2 ± ilmenite, with aeschynite, cerite, hydroxylbastnäsite and hingganite (Text-fig. 5)
↓
Formation of calcite veins and patches (Text-fig. 4)

MINERAL COMPOSITIONS

Chevkinite-(Ce)

Chevkinite is a REE,Ti silicate, with the general formula $A_4BC_2D_2(Si_2O_7)_2O_8$, where A is REE, Ca; B is Fe^{2+}; C is Fe^{2+}, Fe^{3+}, Ti, Al; and D is Ti. Forty-five point analyses of chevkinite-(Ce) in the studied metasomatite may be found in Macdonald *et al*. (2012); they are supplemented by four new determinations in Table 1, where the averages of three types distinguished by degree of brightness on BSE images are also presented. Analytical totals are in the range 97.2–99.5 wt% and the cation sums are very close to stoichiometric (13.0–13.1 apfu). The phase has notably low Ca (0.05-0.23 apfu); high Nd (0.447–0.90 apfu), high Nb (0.083–0.440 apfu), low Th (0.007–0.062 apfu) and low Al (near or below the limit of detection). The average composition is

$(LREE_{3.77}HREE_{0.11}Ca_{0.08})_{3.96}Fe^{2+}(Fe^{2+}_{1.10}Ti_{0.39}Nb_{0.33}Mn_{0.15})_{1.97}Ti_2(Si_{2.00}O_7)O_8$.

In detail, there are slight compositional differences related to variations in brightness on BSE images. Compared to brighter areas, darker areas have higher Ti, Th, La, Y, Ca and Sr contents, and lower Nb, Nd, Sm, Gd and Fe contents. Si and Ce abundances are similar in both types. The enrichment of Ti, and of HREE relative to LREE, and decreased Fe contents, in chevkinite have been related by Jiang (2006), Vlach and Gualda (2007) and Bagiński *et al.* (2015) to hydrothermal alteration. During that process, however, Nb tends to increase and the La/Ce ratio decreases, features not seen in the study samples. Furthermore, the analytical totals and cation sums provide no evidence for hydrothermal alteration; the compositional variations almost certainly reflect primary zonation, related perhaps to the low mobility of the high-valency components and/or a lack of post-crystallization equilibration.

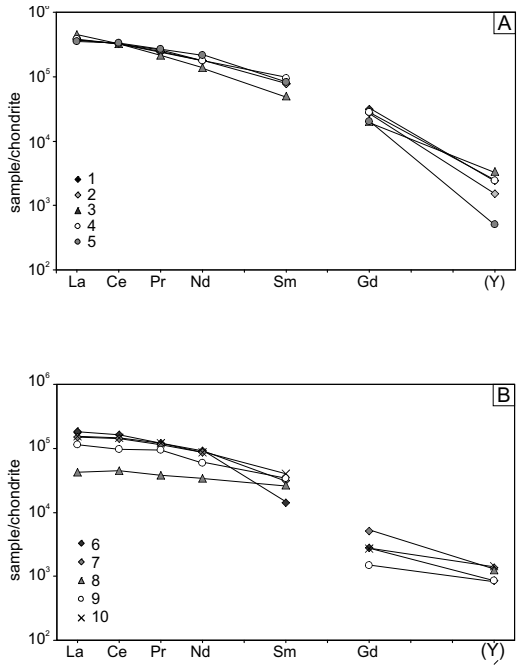

Text-fig. 7. Chondrite-normalized REE patterns for **(A)** chevkinite-(Ce) and **(B)** epidote group minerals. Normalizing factors were used from Sun and McDonough (1989). Data sources: patterns 1-3, averages of brighter, intermediate and darker regions in chevkinite-(Ce), from data in Macdonald *et al*. (2012); 4, 5, Table 1; patterns 6-10, Supplementary Table 1A, analyses 1, 2, 5, 9 and 10

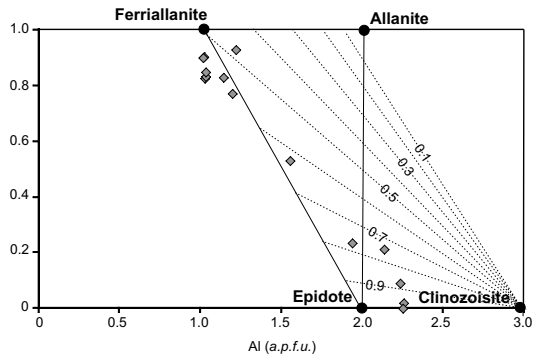

Text-fig. 8. Epidote group minerals plotted in the (REE+Y+Th+Mn+Sr) *v*. Al diagram of Petrik *et al.* (1995), contoured with isolines of the ratio $Fe^{3+}/(Fe^{3+} + Fe^{2+})$. The general increase in oxidation ratio from ferriallanite-(Ce) to epidote calculated from charge balance in generally keeping with the ratios indicated by the isolines. Data from Supplementary Table 1a

The four chondrite-normalised REE patterns shown in Text-fig. 7A all show strong LREE enrichment ([La/Y] ≥79), the crossing of patterns reflects the compositional zoning described above.

Epidote group minerals

Fourteen analyses of epidote group minerals are given in Supplementary Table 1A, with representative analyses in Table 2. Nomenclature and the calculation of structural formulae and oxidation ratios follow the recommendations of Armbruster *et al*. (2006). The phase in the main alteration zone is ferriallanite-(Ce). It contains 0.76–0.92 (apfu) REE+Y and a significant Ti component (0.24–0.27 apfu). The mineral in the dark grey, patchy replacement zone (Text-fig. 4) is compositionally intermediate between ferriallanite and epidote, with 0.21–0.23 REE (apfu) and a reduced Ti content 0.05–0.09 (apfu). The late, very dark grey phase is epidote with a significant clinozoisite (up to 25%) component. The main compositional variations are summarised on Text-fig. 8. With decreasing ΣREE, the La/Y ratio also drops. Chondrite-normalised REE patterns (Text-fig. 7B) are all strongly LREE-enriched and show small Ce anomalies (Ce/Ce* 0.96–1.11). The oxidation ratios ($Fe^{3+}/Fe^{2+}+ Fe^{3+}$) show a strong positive correlation with Ca+Al content, rising from 0.22–0.37 in the ferriallanite-(Ce) to 0.81-0.98 in the clinozoisite-rich epidotes.

TiO_2, ilmenite and titanite

Compositions of TiO_2 intergrown with titanite ± ilmenite (Text-figs 4, 5) are given in Table 3 and Supplementary Table 1B. The TiO_2 is close to end-member composition, with only minor Fe^{2+} (≤0.073 apfu) and Nb (≤0.045 apfu) contents. The ilmenite in the intergrowths is also close to its end-member, $FeTiO_3$, but with significant Mn (≤0.102 apfu; ≤4.65 wt% MnO). The titanite has average composition $Ca_{1.05}Ti_{0.92}Si_{1.00}$, with minor contents of REE (0.03 apfu; 2.9 wt% REE_2O_3) and Nb, Fe^{3+} and Al (≤0.05 apfu). Fluorine levels are up to 0.62 wt. %.

Fergusonite and aeschynite

It is commonly difficult in the metasomatite to distinguish Nb-oxides crystallized at the same time as the chevkinite-(Ce) and those which were formed during later alteration events. Here, the larger crystals such as those in Text-figs 4 and 6 are taken to be early, whilst smaller anhedral grains are considered to have formed later. Representative compositions are presented in Table 4; the full data set is in Supplementary Table 2. The large euhedral crystal shown in Text-fig. 4 is fergusonite-(Y). A profile along the length of the crystal shows significant changes in Ca and Th abundances, with the latter reaching 0.1 apfu, and in the LREE; a possible substitution mechanism is $Ca^{2+} + Th^{4+} = 2REE^{3+}$. Other

primary phases are fergusonite-(Nd), in one case zoned to fergusonite-(Ce) (Fig. 6A), and in another to aeschynite-(Y) (Text-fig. 6B). Late-stage phases are predominantly aeschynite-(Ce).

The chondrite-normalised REE patterns for fergusonite-(Nd) increase from La to Nd, have significant negative Eu anomalies (Eu/Eu* 0.40-0.68) and then decline through the HREE (Text-fig. 9; patterns 5 and 9). There is some variability, e.g. $[La/Yb]_{CN}$ ranges from 3.7–7.4 and the small positive Ce anomalies (Ce/Ce*) range from 1.07-1.17. The patterns for fergusonite-(Y) are HREE-enriched ($[La/Yb]_{CN}$ 0.07–0.27) and with variable Eu anomalies (Eu/Eu* 0.71–2.0) and Ce anomalies (Ce/Ce* 0.63-1.50). The pattern for aeschynite-(Y) is similar to that for fergusonite-(Y) but at higher levels of LREE. Aeschynite-(Ce) shows strong decreases from La to Sm; heavier REE are below levels of detection. One point analysis of fergusonite-(Nd) is unusually Th-rich (8.44 wt% ThO_2); an analysis of fergusonite-(Y) is W-rich (3.69 wt%) WO_3).

The zoned mineral shown in Text-fig. 6B provides information on the compositional changes during alteration of fergusonite-(Nd). The material which is darker on the BSE image (aeschynite-(Y)) and which appears to be replacing the lighter material, has higher Nb, Ca, Ti, Yb, Ta, Y and lower Nd, Sm, Pr, Th, La, Ce, W, Si. The chondrite-normalised REE patterns cross at Tb (Text-fig. 9) and Y becomes the dominant REE.

Cerite-(Ce)

In Table 5 and Supplementary Table 1C are presented analyses of cerite-(Ce) intergrown with allanite in the main allanite zone (Text-fig. 5B), and anhedral

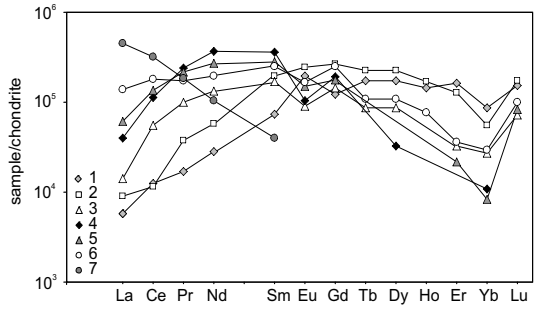

Text-fig. 9. Chondrite-normalized REE patterns for fergusonite and aeschynite. Patterns 4, 5, fergusonite-(Nd); 1, 2, fergusonite-(Y); 6, fergusonite-(Ce); 3, aeschynite-(Y); 7, aeschynite-(Ce). Fergusonite-(Nd) and fergusonite-(Y) predictably show different LREE/HREE relationships; both show variable Ce and Eu anomalies. REE heavier than Sm are below detection in aeschynite-(Ce). Data source: Table 4. Normalizing factors were used from Sun and McDonough (1989). Y proxies for Ho

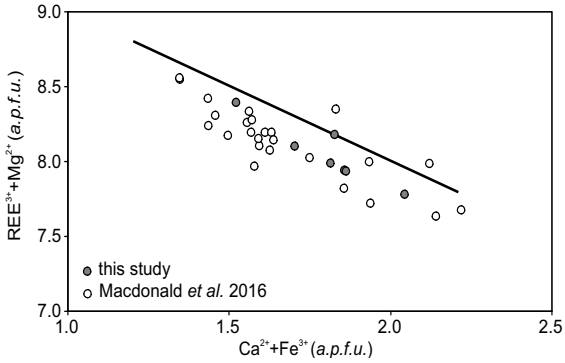

Text-fig. 10. (Mg^{2+}+REE^{3+}) – (Fe^{3+}+Ca^{2+}) plot for cerite-(Ce). The solid line is for cerite–(Ce) from the Norberg district, Bergslagen mining region, Sweden (Holtstam and Andersson 2007). Cerite-(Ce) from this study and in a quartz-epidote metasomatite from further south along the Western zone, Tsakhirin Khuduk occurrence (Macdonald *et al*. 2016), plot close to that trend

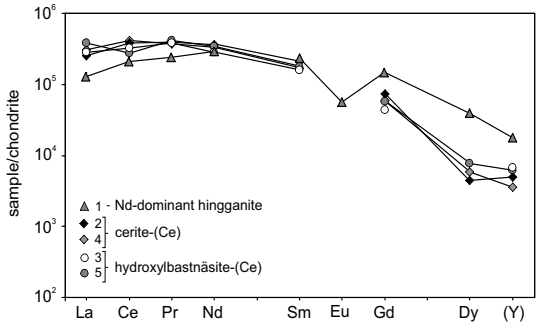

Text-fig. 11. Chondrite-normalised plots for cerite-(Ce), hydroxylbastnäsite-(Ce) and Nd-dominant hingganite. Data sources: Supplementary Table 1C: cerite-(Ce), patterns 2, 4 (analyses 2, 3); hydroxylbastnäsite-(Ce), patterns 3, 5 (analyses 11, 12); Nd-dominant hingganite, pattern 1 (analysis 8). Normalizing factors from Sun and McDonough (1989). Y proxies for Ho

grains close to boundaries between chevkinite and allanite (Text-fig. 5A). Oxide totals are in the range 94.85–97.91 wt% (average 95.83 wt%), the deficit being due mainly to the non-determination of water. Structural formulae have been calculated on the basis of 17 cations. Compositional variation is small; the sum of (REE+Y+Ca), for example, ranges from 9.01–9.07 apfu. Magnesium and Fe^{3+} abundances range from 0.32–0.45 apfu and 0.34-0.62 apfu, respectively. The phase is F-bearing (≤0.77 apfu; ≤0.81 wt%).

Chondrite-normalised REE patterns (Text-fig. 11) show strong, but variable LREE enrichment ($[La/Y]_{CN}$ 47-199) and some variation within the LREE) $[La/Nd]_{CN}$ 0.7–1.4). Positive Ce anomalies are higher (Ce/Ce* 1.15–1.32) than those in chevkinite-(Ce) and the epidote group minerals.

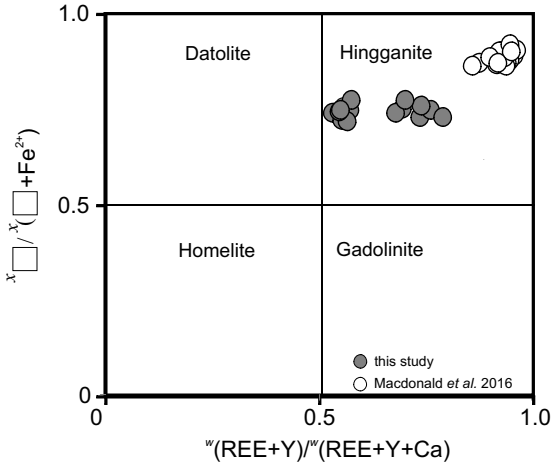

Text-fig. 12. Classification plot for hingganite (solid circles). The data form two groups, with lower and higher values of $^{w}(REE+Y)/^{w}(REE+Y+Ca)$. Also shown is hingganite from a metasomatite located further south in the Western zone (Macdonald *et al*. 2016)

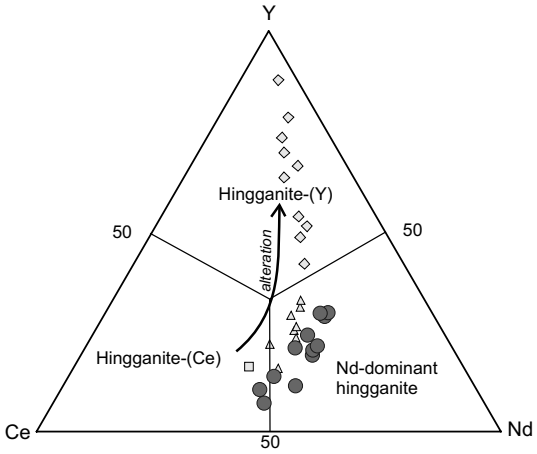

Text-fig. 13. Y-Ce-Nd plot to show that the hingganites (closed circles) lie on a trend parallel to, but slightly displaced from, the trend for the hingganites from the more southerly metasomatite in the Western zone (diamonds, triangles and square; Macdonald *et al.* (2016). Both data sets start just within the hingganite-(Ce) field and with progressive alteration show Nd enrichment. The study suite did not progress into the hingganite-(Y) field

Hingganite

The general formula for hingganite is $(REE,Y)_2Be_2Si_2O_8(OH)_2$. Compositions of hingganite in the metasomatite are given in Table 5 and Supplementary Table 1C. Lacking data for H_2O, formulae were calculated on the basis of Si = 2 apfu. Beryllium has been assumed to be 2 apfu. The majority of analyses are of Nd-dominant hingganite but two are hingganite-(Ce). The phase is Fe-poor (0.23–0.28 apfu) and the $^{x}\square/(^{x}\square + Fe^{2+})$ ratios correspondingly high (0.72–0.77). The Ca content is relatively high (0.42–0.84 apfu), indicating a significant datolite component, and is significantly higher than that in hingganite in the ore-rich metasomatite from the Western zone (0.10-0.26 apfu; Macdonald *et al*. 2016) (Text-fig. 12). Fluorine levels are low (≤ 0.26 wt.%). The sum of (Ca+REE+Y) is, with one exception, in the range 1.67–1.79 apfu, indicating partial vacancies in the W site. The exception has a value of 2.29 apfu and also has low SiO_2, FeO* and CaO contents, a very low analytical total (80.6 wt.%) and high REE contents; it is possibly an altered variety of the hingganite or a mixture of hingganite and unspecified alteration products. The chondrite-normalised REE patterns indicate a sharp increase from La to Sm and then a decrease to the HREE (Text-fig. 11). There are significant positive Ce anomalies (Ce/Ce* 1.2–1.8) and negative Eu anomalies (Eu/Eu* 0.13–0.36).

In detail, there is a compositional range between a higher and a lower Ca types, the higher Ca variety containing lower LREE but more Y and HREE. The higher Ca type appears darker on BSE images, and seems to replace the lighter (Text-fig. 5B). The spread of data on a triangular plot of Y-Ce-Nd (Text-fig. 13) shows a trend similar to, but slightly displaced from, the alteration trend shown by hingganite from the metasomatite of the Western zone studied by Macdonald *et al*. (2016).

REE carbonates

REE-carbonates occur as anhedral grains growing along zone boundaries in allanite (Text-fig. 5A) and as patches and veinlets. The four available analyses are of hydroxylbastnäsite-(Ce), with average composition $(LREE_{0.65}Ca_{0.23}HREE_{0.04}Sr_{0.0.02})_{0.94}(CO_3)(OH_{0.92}F_{0.08})$ (Table 5; Supplementary Table 1C). There is a small variation in the proportions of the LREE, e.g. La/Ce (atomic) 0.30–0.55 and a significant Ca content (0.21–0.24 apfu). Cerium anomalies range from positive to negative (Ce/Ce* 0.68–1.30) (Text-fig. 10). Fluorine levels are low (<0.1 apfu).

Thorite

The compositions of thorite occurring as a small anhedral grain in chevkinite-(Ce) and as a stringer in comb cerite (Text-fig. 5B) are presented in Table 6. The analytical totals range from 82.73–95.92 wt.% and decreasing totals are accompanied by higher Ca,

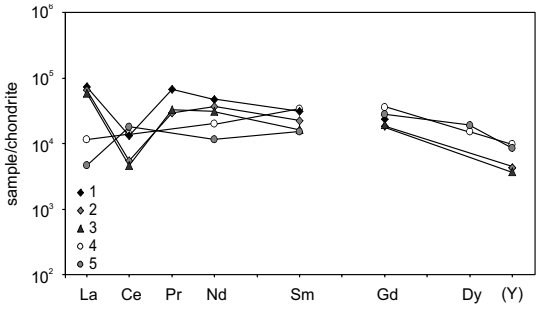

Text-fig. 14. Chondrite-normalized REE patterns for thorite. The slight differences in the patterns possibly reflect the variability of fluid compositions during alteration of the thorite. Data source for patterns 1 to 5: Table 6, analyses 3, 5, 4, 2 and 1. Normalizing factors were used from Sun and McDonough (1989). Y proxies for Ho

La, P, Pr, Nd, Fe, Al, Mg, and lower Si, Th, U, Pb, Ce, Gd, Dy and Y, contents. The low totals are interpreted as either the result of metamictization, especially in the grain enclosed in unaltered chevkinite which may have been protected from strong alteration, and/or alteration by hydrothermal fluids with the addition of water species.

The composition taken to be closest to the unaltered phase (Table 6) has modest U (3.89 wt.% UO_2) and REE (5.22 wt.% REE_2O_3) and low Pb (1.36 wt.% PbO), contents. With progressive alteration, there is a notable increase in P abundance, up to 7.79 P_2O_5 wt.%. Whilst secondary fluorescence of the electron beam by the host cerite-(Ce) may be suspected, it may be noted that the cerite-(Ce) contains only ≤0.6 wt.% P_2O_5 (Table 5). The Th/U increases from 17–119. Chondrite-normalised REE patterns are slightly variable; two point analyses within the same grain show different patterns (Text-fig. 14, patterns 4, 5). A notable feature of the alteration (patterns columns 1–3) is the strong depletion in Ce relative to other LREE, resulting in a significant negative Ce anomaly (Ce/Ce* <0.2) (Fig. 14). There are order of magnitude increases in $[La/Gd]_{CN}$ and $[La/Y]_{CN}$ ratios, indicating the preferential removal of HREE during alteration.

DISCUSSION

Sequence of mineral assemblages

Formation of the peralkaline granite pegmatite involved the crystallization of chevkinite-(Ce), ferriallanite-(Ce) and fergusonite-(Nd). During the initial metasomatism of the pegmatite, chevkinite-(Ce) recrystallization was followed by that of ferriallanite-(Ce), a possible reaction being:

$(LREE_{3.9}Ca_{0.1})(Fe_{2.1}Ti_{2.5}Nb_{0.3})Si_4O_{22} + 1.1Ca^{2+} + 1.1Al^{3+} + H^+ \rightarrow$
$(Ca_{1.2}LREE_{0.8})(Fe^{2+}_{1.8}Al_{1.1}Ti_{0.3})_{3.2}Si_3O_{18}(OH) + 3.1$ $LREE^{3+} + 0.3\ Fe^{2+} + 2.2Ti^{4+} + Si^{4+} + 0.3Nb^{5+} + 3O^{2-}$

(2) The ferriallanite was in turn replaced by epidote:
$(Ca_{1.2}LREE_{0.8})(Fe^{2+}_{1.8}Al_{1.1}Ti_{0.3})_{3.2}Si_{3.1}O_{18}(OH) + 0.5Ca + 0.8Al \rightarrow$
$(Ca_{1.7}LREE_{0.3})(Al_{1.9}Fe^{2+}_{1.2}Ti_{0.1})Si_{3.1}O_{18}(OH) + 0.5LREE + 0.6\ Fe^{2+} + 0.2Ti^{4+}$

In the following, lower-temperature alteration, chevkinite-(Ce) was altered to titanite + TiO_2 (Macdonald *et al*. 2016):
$REE_4Fe_2Ti_3Si_4O_{22} + 2CaO \rightarrow 2CaTiSiO_5 + TiO_2 + 2REE_2O_3 + 2FeO + 2SiO_2$

Locally, TiO_2 reacted with released Fe to form ilmenite. The REE, Fe and Ca released during stages 1 to 3, augmented by a further input of Ca, plus some Mg, Be and water, generated cerite-(Ce), hydroxylbastnäsite-(Ce) and Nd-dominant hingganite. A possible exchange mechanism for cerite, proposed by Holtstam and Andersson (2007) for cerite–(Ce) from the Norberg district, Bergslagen mining region, Sweden, is $(Fe^{3+} + Ca^{2+}) = (Mg^{2+} + REE^{3+})$ (Text-fig. 10). This mechanism applies also to cerite-(Ce) from a more ore-rich metasomatite of the Western ore zone (Macdonald *et al*. 2016) and to the cerite-(Ce) from the current study.

During alteration of chevkinite-(Ce), Nb was released into the fluids and remained there until it entered aeschynite and, to a lesser extent, TiO_2 and titanite. Thorium entered into ferriallanite-(Ce), less so into epidote, and eventually partitioned into aeschynite, hydroxylbastnäsite-(Ce) and thorite. The sequence chevkinite – ferriallanite – epidote involved a decrease in REE+Y concentrations, the elements again entering the accessory minerals in the titanite-TiO_2 zones. Generally, there were decreases in LREE relative to HREE and Y as alteration of the metasomatite proceeded.

As noted by Macdonald *et al.* (2016), the Haldzan-Buragtag deposit has certain features in common with other peralkaline granitic intrusions which host significant abundances of rare-metal minerals, such as Amis, Namibia (Schmitt *et al*. 2002), Tamazeght, Morocco (Salvi *et al*. 2000), Strange Lake, Canada (Salvi and Williams-Jones 2006; Gysi *et al*. 2013), and Khan Bogd, Mongolia (Kynický *et al*. 2011). These features include evidence for the presence of late-stage Ca and HREE metasomatism.

Nature of hydrothermal fluids

Macdonald *et al.* (2016) interpreted studies by Andreev *et al.* (1994) of aqueous CO_2-bearing, Liquid+Vapour inclusions in quartz and epidote in the

metasomatites to suggest that an ore-rich metasomatite closer to the granite body formed at 318–446°C, that being the temperature range of chevkinite recrystallization and growth. Later alteration, i.e. the stage of chevkinite alteration, took place at ~160°C. These may be taken as maximum temperatures for the metasomatite studied here.

There are three lines of evidence concerning the fO_2 during the metasomatism. (i) The calculated oxidation ratios indicate that the fluids became increasingly oxidised during replacement of ferriallanite-(Ce) by epidote. (ii) The calculated ilmenite-TiO_2 reaction is between the Ni-NiO and MH buffers (Zhao *et al.* 1999), suggesting that, during formation of the TiO_2-titanite zones the fO_2 was relatively high but less than the MH buffer. The local presence of ilmenite may point to lower fO_2 condition there, consistent with the relatively high Mn content (≤4.65 wt.% MnO) (Cassidy *et al.* 1988). (iii) The increasingly large positive Ce anomalies found in the phases during successive alteration stages may be taken to be a result of oxidising conditions affecting the valency of Ce (Gieré and Sorensen 2004; Pettke *et al.* 2005; Mayer *et al.* 2014; Berger *et al*. 2008; Uher *et al*. 2009). However, the anomalies may equally be related to preferential partitioning of Ce into the fluids.

Composition of fluids

There was an important role for Ca in the fluids. The replacement of ferriallanite by epidote points to increased Ca activity (cf. Poitrasson 2002; Jiang 2006; Vlach and Gualda 2007; Vlach 2012). As the temperature decreased, the Ca activity in the fluid increased, initiating epidote crystallization. The presence of CO_2 in fluid inclusions in quartz and epidote in the metasomatites (Andreev *et al.* 1994) indicates that the fluids were CO_2-bearing. As a measure of the amount, Rolland *et al*. (2003) suggested that hydrothermal fluids with high XCO_2 (0.2–0.8) are associated with bastnäsite with high La/Nd ratios (~4-5), whereas bastnäsite formed from fluids with very low CO_2 contents has low La/Nd (0.6–2). On that basis, the La/Nd ratios of the hydroxylbastnäsite in the studied metasomatite (0.53–0.63) would indicate a small CO_2 component in the fluids, consistent with the relatively low modal amount of REE-carbonate. These observations are consistent with the experimental results of Wang *et al*. (2001) who showed that titanite is stable under relatively low fCO_2 conditions, being replaced at higher fCO_2 by rutile and carbonate. The latest stage carbonate was calcite (Text-fig. 4), indicating that the REE had by then been depleted in the fluids.

Several points indicate that activity of F was low. (a) The relatively low F content of both the hydroxylbastnäsite-(Ce) and cerite-(Ce). (b) F in the hingganite is below detection and fluorite is absent. (c) Retention of Nb in the system, as aeschynite and to a minor extent in TiO_2 and titanite, is consistent with a low F content in the fluid; the solubility of Nb_2O_5 (solid) in aqueous fluids increases with increasing HF concentration, as shown experimentally by Timofeev *et al.* (2015).

Changes in fluid composition

Field and petrographic studies have shown that in the Western zone the degree of metasomatism increased, and the content of rare-metal minerals decreased, to the north, that is away from the intrusive mass into the host rocks. One indicator of the change is the size of the recrystallized chevkinite crystals, from up to 8 × 2-3 cm (sample chev7; Macdonald *et al*. (2016)) to 2 × 0.3 cm (this study). Apart from the hingganite in K6 having higher Ca contents than in chev7, there are no major differences in composition of the mineral phases. It appears that the metasomatising fluids in both parts of the Western zone were broadly similar.

The source of the hydrothermal fluids is unknown. However, formation of the pre-metasomatism pegmatites was followed by at least five more episodes of tectono-magmatic events, including late intrusions of basalt (Kovalenko *et al.* 1995). The basaltic magmas may have been the source of low temperature fluids with the simple composition H_2O-Ca-CO_3.

Acknowledgements

For assistance during microprobe analyses, we thank Lidia Jeżak and Dr Piotr Dzierżanowski, our close collaborator and friend who passed away on December 31st, 2015. We also thank Harvey Belkin, Pavel Uher and Dmitry Zozulya for very helpful reviews of the manuscript. This work was financially supported by IGMiP grant BSt 173504/39/2015.

REFERENCES

Andreev, G.V. and Ripp, G.S. 1996. Rare-metal epidote-quartz metasomatites of the Khaldzan Buregteg massif. *Proceedings of the Russian Mineralogical Society*, **125**, 24–30. [In Russian]

Andreev, G.V., Ripp, G.S., Sharakshinov, A.O. and Minin, A.D. 1994. Rare-metal Mineralization in Alkaline Granitoids of Western Mongolia, pp. 1–137. BNTS SO RAN, Ulan Ude. [In Russian]

Armbruster, T., Bonazzi, P., Akasaka, M., Bermanec, V.,

Chopin, C., Giere, R., Heuss-Assbichler, S., Liebscher, A., Menchett,e, S., Pan, Y. and Pasero, M. 2006. Recommended nomenclature of epidote-group minerals. *European Journal of Mineralogy*, **18**, 551–567.

Bagiński, B., Macdonald, R., Dzierżanowski, P., Zozulya, D. and Kartashov, P.M. 2015. Hydrothermal alteration of chevkinite-group minerals: products and mechanisms. Part 1. Hydration of chevkinite-(Ce). *Mineralogical Magazine*, **79**, 1019–1037.

Bagiński, B., Zozulya, D., Macdonald, R., Kartashov, P. and Dzierżanowski, P. 2016. Low-temperature hydrothermal alteration of a rare-metal rich quartz-epidote metasomatite from the El'ozero deposit, Kola Peninsula, Russia. *European Journal of Mineralogy*. DOI: 10.1127.ejm/2016/0028-2552.

Berger, A., Gnos, E., Janots, E., Fernandez, A. and Giese, J. 2008. Formation and composition of rhabdophane, bastnäsite and hydrated thorium minerals during alteration: implications for geochronology and low-temperature processes. *Chemical Geology*, **254**, 238–248.

Cassidy, K.F., Groves, D.I. and Binns, R.A. 1988. Manganoan ilmenite formed during regional metamorphism of Archean mafic and ultramafic rocks from Western Australia. *The Canadian Mineralogist*, **26**, 999–1012.

Gieré, R. and Sorensen, S.S. 2004. Allanite and other REE-rich epidote group minerals. In: A. Liebscher and G. Franz (Eds), Epidotes. *Reviews in Mineralogy and Geochemistry*, **56**, 431–493.

Gramaccioli, C.M., Diella, V. and Demartin, F. 1999. The role of fluoride complexes in REE geochemistry and the importance of 4f electrons: some examples in minerals. *European Journal of Mineralogy,* **11**, 983–992.

Gysi, A.P. and Williams-Jones, A.E. 2013. Hydrothermal mobilization of pegmatite-hosted REE and Zr at Strange Lake, Canada: A reaction path model. *Geochimica et Cosmochimica Acta*, **122**, 324–352.

Holtstam, D. and Andersson, U.B. 2007. The REE minerals of the Bastnas-type deposits, south-central Sweden. *The Canadian Mineralogist*, **45**, 1073–1114.

Jarosewich, E and Boatner, L.A. 1991. Rare-earth element reference samples for electron microprobe analysis. *Geostandards Newsletter*, **15**, 397–399.

Jiang, N. 2006. Hydrothermal alteration of chevkinite-(Ce) in the Shuiquangou syenitic intrusion, northern China. *Chemical Geology*, **227**, 100–112.

Kartashov, P.M. 1994. Zr- and Nb-bearing varieties of chevkinite-(Ce) and their alteration products, first occurrence in Mongolia. Ninth IAGOD Symposium, Beijing, 2, 696–697.

Kartashov, P.M., Voloshin, A.V., and Pakhomovsky, Ya.A. 1993. Zonal crystalline gadolinite from alkali granite pegmatitesof the Khaldzan–Buregtega (Mongolian Altai), *Zapiski Vsesoyuznogo Mineralogicheskogo Obshchestva,* **122**, 65–79.

Kartashov, P.M., Ferraris, G., Ivaldi, G., Sokolova, E. and McCammon, C.A. 2002. Ferriallanite-(Ce), $CaCeFe^{3+}AlFe^{2+}(SiO_4)(Si_2O_7)O(OH)$, a new member of the epidote group: description, X-ray and Mössbauer study. *The Canadian Mineralogist*, **40**, 1641–1648.

Kovalenko, V.I., Tsaryeva, G.M., Goreglyad, A.V., Yarmolyuk, V.V., Troitsky, V.A., Hervig, R.L., and Farmer, G.L. 1995. The peralkaline granite-related Khaldzan-Buregteg rare metal (Zr, Nb, *REE*) deposit, Western Mongolia. *Economic Geology*, **90**, 530–547.

Kovalenko, V.I., Goregylad ,A.V. and Tsaryeva, G.M. 1985. Khadzan Buregtey massif – a new manifestation of rare-metal peralkaline granitoids of MPR. *Doklady Akademii Nauk SSSR* **280**, 954–959. [In Russian]

Kynický, J., Chakhmouradian, A.R., Xu C., Krmiček, L. and Galiová, M. 2011. Distribution and evolution of zirconium mineralization in peralkaline granites and associated pegmatites of the Khan Bogd complex, southern Mongolia. *The Canadian Mineralogist*, **49**, 947–965.

Liferovich, R.P. and Mitchell, R.H. 2005. Composition and paragenesis of Na-, Nb- and Zr-bearing titanite from Khibina, Russia, and crystal-structure data for synthetic analogues. *The Canadian Mineralogist*, **43**, 795–812.

Lumpkin, G.R., Blackford, M.G. and Colella, M. 2013. Chemistry and radiation effects of davidite. *American Mineralogist*, **98**, 275–278.

Macdonald, R., Bagiński, B., Kartashov, P., Zozulya, D. And Dzierżanowski, P. 2012. Chevkinite-group minerals from Russia and Mongolia: new compositional data from metasomatites and ore deposits. *Mineralogical Magazine*, **76**, 535–549.

Macdonald, R., Bagiński, B., Kartashov, P.M., Zozulya, D. and Dzierżanowski, P. 2015a. Hydrothermal alteration of chevkinite-group minerals. Part 2. Metasomatite from the Keivy massif, Kola Peninsula, Russia. *Mineralogical Magazine*, **79**, 1039–1059.

Macdonald, R., Bagiński, B., Kartashov, P.M., Zozulya, D. and Dzierżanowski, P. 2015b. Hydrothermal alteration of a chevkinite-group mineral to a bastnasite-(Ce)-ilmenite-columbite-(Fe) assemblage: interaction with a F, CO_2-rich fluid. *Mineralogy and Petrology*, **109**, 659–678.

Macdonald, R., Bagiński, B., Kartashov, P.M., Zozulya, D. and Dzierżanowski, P. 2016. Interaction of rare-metal minerals with hydrothermal fluids; evidence from quartz-epidote metasomatites of the Haldzan Buragtag massif, Mongolian Altai. *The Canadian Mineralogist*

Mayer, B.S., Krenn, E. and Finger, F. 2014. Microcrystals of Th-rich monazite (La) with a negative Ce anomaly in metadiorite and their role for documenting Cretaceous metamorphism in the Slavonian Mountains (Croatia). *Mineralogy and Petrology*, **108**, 231–243.

Pan, Y., Fleet, M.E. and MacRae, N.D. 1993. Late alteration in titanite ($CaTiSiO_5$): redistribution and remobilization of rare earth elements and implications for U/Pb and Th/Pb geochronology and nuclear waste disposal. *Geochimica et Cosmochimica Acta*, **57**, 355–367.

Petrik, I., Broska, I., Lipka; J. and Siman, P. 1995. Granitoid allanite-(Ce) substitution relations, redox conditions and REE distributions (on an example of I-type granitoids, Western Carpathians, Slovakia). *Geologica Carpathica,* **46**, 79–94.

Pettke, T., Audetat, A., Schaltegger, U. and Heinrich, C.A. 2005. Magmatic-to-hydrothermal crystallization in the W-Sn mineralized Mole Granite (NSW, Australia). Part II: evolving zircon and thorite trace element chemistry. *Chemical Geology*, **220**, 191–213.

Poitrasson, F. 2002. In situ investigations of allanite hydrothermal alteration: examples from calc-alkaline and anorogenic granites of Corsica (southeast France). *Contributions to Mineralogy and Petrology*, **142**, 485–500.

Pouchou, J.L. and Pichoir, J.F. 1991. Quantitative analysis of homogeneous or stratified microvolumes applying the model 'PAP'. In: Newbury H. (Eds), Electron Probe Quantitation, pp. 31–75. Plenum Press; New York.

Rolland, Y., Cox, S., Boullier, A.-M., Pennacchioni, G. and Mancktelow, N. 2003. Rare earth and trace element mobility in mid-crustal shear zones: insights from the Mont Blanc Massif (Western Alps). *Earth and Planetary Science Letters*, **214**, 203–219.

Salvi, S. and Williams-Jones, A.E. 2006. Alteration, HFSE mineralisation and hydrocarbon formation in peralkaline igneous systems: Insights from the Strange Lake Pluton, Canada. *Lithos*, **91**, 19–34.

Salvi, S., Fontan, F., Monchoux, P., Williams-Jones, A.E. and Moine, B. 2000. Hydrothermal mobilization of high field strength elements in alkaline igneous systems: Evidence from the Tamazeght Complex, Morocco. *Economic Geology*, **95**, 559–576.

Sokolova, E., Hawthorne, F.C., Della Ventura, G. and Kartashov, P.M. 2004. Chevkinite-(Ce): crystal structure and the effect of moderate radiation-induced damage on site-occupancy refinement. *The Canadian Mineralogist*, **42**, 1013–1025.

Sun, S.-S. and McDonough, W.F. 1989. Chemical and isotopic systematics of oceanic basalts: implications for mantle composition and processes. In: A.D. Saunders and M.J. Norry (Eds), Magmatism in the ocean basins. *Geological Society of London Special Publication* **42**, 313–345.

Timofeev, A., Migdisov, A.A. and Williams-Jones, A.E. 2015. An experimental study of the solubility and speciation of niobium in fluoride-bearing aqueous solutions at elevated temperature. *Geochimica et Cosmochimica Acta,* **158**, 103–111.

Uher, P., Ondrejka, M. and Konečný, P. 2009. Magmatic and post-magmatic Y-REE-Th phosphate, silicate and Nb-Ta-Y-REE oxide minerals in A-type metagranite: an example from the Tuřcok massif, the Western Carpathians, Slovakia. *Mineralogical Magazine,* **73**, 1009–1025.

Vlach, S.R.F. 2012. Micro-structural and compositional variations of hydrothermal epidote-group minerals from a peralkaline granite, Corupá Pluton, Graciosa Province, South Brazil, and their petrological implications. *Annals of the Brazilian Academy of Sciences*, **84**, 139–157.

Vlach, S.R.F. and Gualda, G.A.R. 2007. Allanite and chevkinite in A-type granites and syenites of the Graciosa Province, southern Brazil. *Lithos*, **97**, 98–121.

Wand, R.C., Wang, D.Z., Zhao, G.T., Lu, J.J., Chen, X. M. and Xu, S.J. 2001. Accessory mineral record of magma-fluid interaction in the Laoshan I- and A-type granitic complex, Eastern China. *Physics and Chemistry of the Earth*, **A26**, 835–849.

Zhao, D., Essene, E.J. and Zhang, Y. 1999. An oxygen barometer for rutile-ilmenite assemblages: oxidation state of metasomatic agents in the mantle. *Earth and Planetary Letters*, **166**, 127–137.

Manuscript submitted: 16th March 2016
Revised version accepted: 30th June 2016

APPENDIX I Analytical conditions for chevkinite-(Ce)				
Element	Line	Crystal	Standard	Approx. detection limit (wt.%)
Al	Kα	TAP	orthoclase	0.01
Ba	Lα	LiF	barite	0.12
Ca	Lα	PET	$CaSiO_3$	0.01
Ce	Kα	PET	CeP_5O_{14}	0.06
Cl	Lα	PET	Tugtupite	0.02
Dy	Lß	LiF	REE1	0.33
Eu	Lß	LiF	REE2	0.30
Fe	Kα	LiF	hematite	0.04
Gd	Lß	LiF	GdP_5O_{14}	0.19
Hf	Mα	TAP	Hf-SPI	0.03
La	Lα	PET	LaB_6	0.05
Mg	Kα	TAP	diopside	0.01
Mn	Kα	LiF	rhodonite	0.04
Na	Kα	TAP	albite	0.01
Nb	Lα	PET	Nb metal	0.05
Nd	Lß	LiF	NdP_5O_{14}	0.18
P	Kα	PET	Apatite Jap2	0.02
Pr	Lß	LiF	PrP_5O_{14}	0.12
Sc	Kα	PET	Sc metal	0.01
Si	Kα	TAP	Wollastonite	0.01
Sm	Lß	LiF	SmP_5O_{14}	0.19
Sr	Lα	TAP	$SrTiO_3$	0.03
Ta	Mα	TAP	Ta metal	0.04
Tb	Lα	LiF	REE4	0.14
Th	Mα	PET	ThO_2 synthetic	0.09
Ti	Kα	PET	rutile	0.02
U	Mß	PET	vorlanite	0.08
Y	Lα	TAP	$Y_3Al_5O_{12}$	0.04
Yb	Lα	liF	REE3	0.14
Zr	Lα	PET	Zircon ED2	0.05

The codes REE1 to 4 refer to glasses containing REE ($REEPO_4$) (Jarosewich and Boatner 1991)

APPENDIX II TAB. 1-6

wt.%							
Nb_2O_5	3.22	3.62	3.59	0.63	3.60	3.29	1.63
Ta_2O_5	0.12	0.17	0.23	0.17			
P_2O_5	bd	bd	bd	bd	0.06	bd	0.04
TiO_2	14.29	13.93	14.09	17.41	14.03	14.36	16.72
ZrO_2	0.26	0.59	0.60	bd	0.50	0.76	0.28
ThO_2	0.19	0.25	0.37	bd	0.38	0.30	0.71
UO_2	0.11	bd	bd	bd	0.15	bd	0.09
SiO_2	18.26	18.21	18.26	18.46	18.13	18.19	18.40
Al_2O_3	bd	bd	bd	0.05	0.02	bd	bd
La_2O_3	10.46	10.65	10.47	9.77	10.20	10.45	12.43
Ce_2O_3	23.6	23.08	23.14	24.19	23.06	23.41	23.16
Pr_2O_3	2.58	2.91	2.68	2.95	2.63	2.77	2.36
Nd_2O_3	9.89	9.63	9.59	11.69	9.67	9.76	7.52
Sm_2O_3	1.17	1.65	1.42	1.44	1.36	1.40	0.88
Gd_2O_3	0.76	0.66	0.77	0.48	0.75	0.64	0.48
Dy_2O_3	bd	bd	0.27	bd	0.43	bd	0.39
Y_2O_3	0.43	0.49	0.50	0.10	0.48	0.31	0.68
FeO*	11.64	11.48	11.30	10.90	11.57	11.56	10.46
MnO	0.72	0.71	0.69	0.26	0.75	0.70	1.05
MgO	bd	bd	bd	0.09	bd	bd	bd
CaO	0.35	0.24	0.26	0.86	0.27	0.29	0.61
SrO	0.06	0.07	0.16	bd	0.40	0.48	0.64
Na_2O	0.06	0.09	0.08	bd	0.10	0.15	0.05
Total	98.17	98.43	98.47	99.45	97.89	98.32	98.09
Formulae on 22 oxygen basis							
Ca	0.083	0.057	0.061	0.199	0.064	0.068	0.142
Sr	0.008	0.009	0.020	0.000	0.052	0.061	0.080
Na	0.026	0.038	0.034	0.000	0.035	0.032	0.018
La	0.851	0.866	0.851	0.779	0.832	0.849	0.995
Ce	1.906	1.864	1.868	1.914	1.866	1.888	1.841
Pr	0.207	0.234	0.215	0.232	0.212	0.223	0.186
Nd	0.779	0.758	0.755	0.902	0.764	0.768	0.583
Sm	0.089	0.125	0.108	0.107	0.104	0.106	0.066
Gd	0.056	0.048	0.056	0.034	0.053	0.047	0.034
Dy	0.000	0.000	0.029	0.000	0.002	0.000	0.009
Y	0.050	0.058	0.059	0.011	0.057	0.036	0.079
Th	0.010	0.013	0.019	0.000	0.019	0.015	0.035
U	0.005	0.000	0.000	0.000	0.000	0.000	0.001
Sum *A*	4.070	4.070	4.047	4.178	4.058	4.092	4.069
Fe^{2+} (=B)	1.000	1.000	1.000	1.000	1.000	1.000	1.000
Fe^{2+}	1.148	1.117	1.084	0.970	1.139	1.128	0.900
Mn	0.135	0.133	0.129	0.048	0.140	0.130	0.192
Mg	0.000	0.000	0.000	0.002	0.000	0.000	0.000
Nb	0.321	0.361	0.358	0.062	0.360	0.327	0.160
Ta	0.007	0.010	0.014	0.010			
Zr	0.028	0.065	0.065	0.000	0.054	0.041	0.020
Al	0.000	0.000	0.000	0.002	0.001	0.000	0.000
Ti	0.371	0.310	0.336	0.829	0.332	0.378	0.729
Sum *C*	2.010	1.996	1.985	1.923	2.025	2.004	2.001
Ti (=D)	2.000	2.000	2.000	2.000	2.000	2.000	2.000
P	0.000	0.000	0.000	0.000	0.001	0.000	0.001
Si	4.028	4.016	4.026	3.988	4.006	4.006	3.993
Sum *T*	4.028	4.016	4.026	3.988	4.007	4.006	3.994
Σ cations	13.1	13.1	13.1	13.1	13.1	13.1	13.1

Explanation: 1-4, new analyses, from crystal shown in Fig. 4; 4-6, averages based on BSE intensity-5, bright, 6, intermediate, 7, dark. FeO*, all Fe as Fe^{2+}. bd, below detection; Blank, not determined. Data for 4-6 from Macdonald *et al.* (2012).

Table 1. Compositions of chevkinite-(Ce) in quartz-epidote metasomatite

	1	2	3	4	5	6	7	8
wt.%								
P_2O_5	bd	bd	0.11	bd	0.09	bd	bd	0.04
SiO_2	29.69	30.00	29.60	29.83	32.45	35.97	37.65	37.58
TiO_2	3.54	3.13	3.10	3.36	1.85	0.71	0.05	0.07
ThO_2	0.28	0.17	bd	bd	bd	bd	0.11	bd
Al_2O_3	8.41	9.47	10.09	8.53	13.99	21.18	23.43	23.26
Y_2O_3	0.17	0.31	bd	0.26	0.17	0.07	0.12	bd
La_2O_3	5.09	4.03	6.41	4.37	3.15	1.44	bd	bd
Ce_2O_3	11.58	10.15	12.37	10.58	7.00	3.35	0.10	0.07
Pr_2O_3	1.33	1.66	1.34	1.25	1.05	0.38	bd	bd
Nd_2O_3	4.93	4.89	4.37	5.05	3.22	1.56	bd	bd
Sm_2O_3	0.25	0.57	0.18	0.63	0.61	bd	0.20	bd
Gd_2O_3	0.32	0.37	bd	0.29	0.17	bd	0.19	bd
MgO	0.02	bd	bd	bd	bd	bd	bd	bd
CaO	10.26	10.77	9.44	10.7	14.95	19.74	23.51	23.12
MnO	0.36	0.42	0.44	0.48	0.25	0.06	bd	0.06
FeO*	19.68	19.39	18.18	20.03	17.60	12.41	12.18	12.62
Total	95.91	95.33	95.63	95.36	96.55	96.87	97.54	96.82
Formulae on the basis of ΣA+M+T = 8								
Si	3.016	3.011	3.016	3.012	2.988	3.012	2.984	2.993
Al	0.000	0.000	0.000	0.000	0.012	0.000	0.016	0.007
Sum T	3.016	3.011	3.016	3.012	3.000	3.012	3.000	3.000
Al	1.007	1.120	1.210	1.015	1.504	2.090	2.173	2.176
Ti	0.270	0.236	0.238	0.255	0.128	0.045	0.003	0.004
Mn	0.031	0.036	0.038	0.041	0.019	0.004	0.000	0.004
Fe	1.672	1.628	1.549	1.691	1.355	0.869	0.807	0.841
Mg	0.003	0.000	0.000	0.000	0.000	0.000	0.000	0.000
Sum M	2.983	3.020	3.035	3.003	3.007	3.008	2.983	3.024
Th	0.006	0.004	0.000	0.000	0.000	0.000	0.002	0.000
Y	0.009	0.017	0.000	0.014	0.008	0.003	0.005	0.000
La	0.191	0.149	0.241	0.163	0.107	0.044	0.000	0.000
Ce	0.431	0.373	0.462	0.391	0.236	0.103	0.003	0.002
Pr	0.049	0.061	0.050	0.046	0.035	0.012	0.000	0.000
Nd	0.179	0.175	0.159	0.182	0.106	0.047	0.000	0.000
Sm	0.009	0.020	0.006	0.022	0.019	0.000	0.005	0.000
Gd	0.011	0.012	0.000	0.010	0.005	0.000	0.005	0.000
Ca	1.117	1.158	1.031	1.158	1.475	1.771	1.997	1.973
Sum A	2.001	1.969	1.948	1.985	1.992	1.980	2.017	1.975
REE + Y	0.878	0.807	0.918	0.828	0.517	0.209	0.018	0.002
Ox ratio	0.31	0.34	0.22	0.36	0.52	0.66	0.98	0.94

FeO*, all Fe as Fe^{2+}. bd, below detection. Ox ratio, $Fe^{3+}/(Fe^{3+}+Fe^{2+})$. All samples from epidote group area on Fig. 4.

Table 2. Representative compositions of epidote group minerals

	titanite				rutile			ilmenite		
	1	2	3	4	5	6	7	8	9	10
wt.%										
Nb_2O_5	2.61	2.23	0.34	0.75	7.03	2.56	5.80	0.28	0.41	0.70
SiO_2	29.51	29.62	30.33	29.76	0.48	0.02	0.02	0.06	0.03	bd
TiO_2	35.77	33.17	37.62	34.78	87.66	92.59	91.78	51.53	50.67	51.45
Al_2O_3	0.45	0.97	0.83	0.76	0.06	bd	0.05	bd	bd	bd
Fe_2O_3*	1.78	3.74	0.86	2.84						
Y_2O_3	0.15	bd	0.10	0.20						
Ce_2O_3	0.80	0.61	0.35	0.73						
Nd_2O_3	1.31	0.46	0.47	1.06						
Sm_2O_3	0.26	bd	bd	0.41						
Gd_2O_3	0.26	bd	bd	0.22						
MgO	bd	bd	bd	bd	bd	bd	bd	0.03	0.03	0.03
CaO	26.92	27.85	28.51	27.53	bd	bd	0.22	0.47	0.62	0.16
MnO	bd	bd	bd	bd	bd	bd	bd	2.85	4.65	3.57
FeO*					2.20	1.96	2.26	43.16	41.13	41.48
F	bd	0.43	0.58	0.51						
Sum	99.82	99.08	99.99	99.55	97.43	97.13	100.13	98.38	97.54	97.39
O=F	0.00	0.18	0.24	0.21						
Total	99.82	98.90	99.75	99.34	97.43	97.13	100.48**	98.38	97.54	97.39
	Formulae on basis of 5 oxygens				*on basis of 2 oxygens*			*on basis of 3 oxygens*		
Nb	0.040	0.034	0.005	0.011	0.045	0.016	0.036	0.003	0.005	0.008
Si	0.991	0.996	0.997	0.999	0.007	0.000	0.000	0.002	0.001	0.000
Ti	0.903	0.839	0.930	0.878	0.924	0.968	0.940	0.994	0.987	1.000
Al	0.018	0.038	0.032	0.030	0.001	0.000	0.001	0.000	0.000	0.000
Mg	0.000	0.000	0.000	0.000	0.000	0.000	0.000	0.001	0.001	0.001
Mn	0.000	0.000	0.000	0.000	0.000	0.000	0.000	0.062	0.102	0.078
Fe^{3+}	0.045	0.095	0.021	0.072						
Ce	0.010	0.008	0.004	0.009						
Nd	0.016	0.006	0.006	0.013						
Sm	0.003	0.000	0.000	0.005						
Gd	0.003	0.000	0.000	0.002						
Fe^{2+}					0.026	0.023	0.026	0.926	0.891	0.896
Ca	0.968	1.003	1.004	0.990	0.000	0.000	0.003	0.013	0.017	0.004
Y	0.003	0.000	0.002	0.004						
F	0.000	0.046	0.060	0.054						
Σ cations	3.00	3.02	3.00	3.01	1.00	1.01	1.01	2.00	2.00	1.99

Fe_2O_3*, all Fe as Fe^{3+}. FeO*, all Fe as Fe^{2+}. bd, below detection. Blank, not determined. Analyses 1-4, all from vein on Fig. 4; 5-6, zone on Fig. 5D; 7, vein, Fig. 4; 8-10, zone on Fig. 5D. ** included WO_3 0.16 wt.%.

Table 3. Representative compositions of titanite, rutile and ilmenite

	1	2	3	4	5	6	7	8	9
Species	F-(Y)	F-(Y)	NA-(Y)	F-(Nd)	F-(Ce)	F-(Ce)	F-(Y)	A-(Ce)	F-(Nd)
wt.%									
WO_3	0.71	3.69	0.19	0.37	0.61	bd	bd	bd	bd
Nb_2O_5	47.73	45.01	46.32	43.26	44.25	44.40	41.11	6.80	44.82
Ta_2O_5	0.59	0.70	1.42	0.69	1.15	0.52	3.23	0.52	0.16
SiO_2	0.08	0.53	0.06	0.28	0.08	0.05	0.22	0.06	0.20
TiO_2	0.41	1.61	16.88	1.68	0.40	0.24	1.93	41.63	0.26
ThO_2	0.97	0.26	0.90	3.46	0.50	1.01	6.68	1.76	8.44
UO_2	0.12	bd	bd	0.17	0.13	0.21	0.17	bd	0.13
Al_2O_3	bd	bd	0.04	0.03	0.03	0.03	0.03	0.04	bd
Y_2O_3	21.90	29.50	6.71	5.45	6.10	6.99	14.44	0.42	2.15
La_2O_3	0.25	0.16	0.39	1.70	3.92	3.83	0.43	12.54	1.10
Ce_2O_3	0.83	0.89	3.96	9.69	11.75	12.92	2.12	22.77	8.13
Pr_2O_3	0.42	0.19	1.11	2.42	1.93	1.94	0.82	2.07	2.67
Nd_2O_3	3.14	1.53	7.30	14.92	11.54	10.60	6.05	5.72	20.12
Sm_2O_3	3.49	1.30	3.01	5.00	5.87	4.47	5.65	0.71	6.39
Eu_2O_3	1.66	1.31	0.61	1.00	0.73	1.11	1.23	bd	0.70
Gd_2O_3	6.34	2.91	3.39	4.19	6.10	5.90	6.86	2.57	4.51
Tb_2O_3	0.98	0.75	0.37	bd	0.41	0.47	0.73	bd	bd
Dy_2O_3	5.89	4.44	1.53	1.07	2.05	2.13	3.21	bd	0.96
Ho_2O_3	1.10	0.93	bd	bd	bd	0.50	bd	bd	bd
Er_2O_3	2.42	3.09	0.62	0.41	0.43	0.68	1.28	bd	bd
Yb_2O_3	1.07	1.69	0.53	0.16	0.53	0.57	1.09	bd	0.21
Lu_2O_3	0.50	0.44	0.21	0.24	0.15	0.29	0.43	bd	bd
CaO	0.06	0.06	4.30	1.79	0.49	0.35	0.83	1.12	1.19
MnO	bd	bd	0.05	bd	bd	bd	0.05	bd	bd
FeO*	bd	bd	0.19	0.26	0.15	bd	0.71	0.35	bd
Total	100.66	100.99	100.09	98.24	99.30	99.21	99.30	99.08	102.14
Formulae on the basis of (Nb+Ta+Ti) = 1									
Ca	0.003	0.003	0.135	0.091	0.025	0.018	0.043	0.035	0.062
La	0.004	0.003	0.004	0.030	0.070	0.069	0.008	0.134	0.020
Ce	0.014	0.015	0.043	0.169	0.209	0.232	0.037	0.242	0.145
Pr	0.007	0.003	0.012	0.042	0.034	0.035	0.014	0.022	0.047
Nd	0.051	0.025	0.077	0.254	0.200	0.186	0.103	0.059	0.350
Sm	0.055	0.021	0.030	0.082	0.098	0.076	0.093	0.007	0.107
Eu	0.026	0.021	0.006	0.016	0.012	0.019	0.020	0.000	0.012
Gd	0.095	0.044	0.033	0.066	0.098	0.096	0.109	0.025	0.073
Tb	0.015	0.011	0.004	0.000	0.007	0.008	0.011	0.000	0.000
Dy	0.086	0.066	0.014	0.016	0.032	0.034	0.049	0.000	0.015
Ho	0.016	0.014	0.000	0.000	0.000	0.008	0.000	0.000	0.000
Er	0.034	0.045	0.006	0.006	0.007	0.010	0.019	0.000	0.000
Yb	0.015	0.024	0.005	0.002	0.008	0.009	0.016	0.000	0.003
Lu	0.007	0.006	0.002	0.003	0.002	0.004	0.006	0.000	0.000
Y	0.529	0.722	0.105	0.138	0.157	0.182	0.367	0.006	0.056
Th	0.010	0.003	0.006	0.037	0.006	0.011	0.073	0.012	0.094
U	0.001	0.000	0.000	0.002	0.001	0.002	0.002	0.000	0.001
W	0.005	0.025	0.001	0.003	0.004	0.000	0.000	0.000	0.000
Fe^{2+}	0.000	0.000	0.005	0.010	0.006	0.000	0.028	0.008	0.000
Mn	0.000	0.000	0.001	0.000	0.000	0.000	0.002	0.000	0.000
Al	0.000	0.000	0.001	0.002	0.002	0.002	0.002	0.001	0.000
Nb	0.979	0.936	0.616	0.931	0.970	0.984	0.889	0.089	0.988
Ta	0.007	0.009	0.011	0.009	0.015	0.007	0.042	0.004	0.002
Ti	0.014	0.056	0.373	0.060	0.015	0.009	0.069	0.907	0.010
Si	0.004	0.024	0.002	0.013	0.004	0.002	0.011	0.002	0.010

Explanation: Analyses 1, 2, in cluster in titanite -TiO_2 zone, Fig. 5d; 3, 4, darker and brighter components in rounded prism, Fig. 6b; 5, 6, in skeletal prism (Fig. 6a); 7, 8, anhedral grains in titanite-TiO_2 zone, Fig. 5d; euhedral grain in chevkinite FeO*, all Fe as Fe^{2+}; bd, below detection. F-(Y), fergusonite-(Y); F-(Nd), fergusonite-(Nd); A-(Y), aeschynite-(Y); F-(Ce), fergusonite -(Ce); A-(Ce), aeschynite-(Ce); NA-(Y), nioboaeschynite-(Y)

Table 4. Compositions of Nb oxides

	cerite-(Ce)				hingganite			hydroxylbastnasite-(Ce)		
	1	2	3	4	5	6	7	8	9	10
P_2O_5	0.57	0.50	0.57	0.21		0.49	bd			
SiO_2	21.81	21.68	21.83	21.62	29.25	26.04	30.01	1.85	1.25	1.13
TiO_2	0.23	0.20	0.26	0.27	0.12	0.11	0.08			
ThO_2					0.14	0.85	0.16	1.27	1.38	1.18
Al_2O_3	0.32	0.33	0.21	0.07	bd	0.39	bd			
Y_2O_3	1.07	0.72	0.92	0.35	5.14	2.45	3.94	1.76	1.30	1.25
La_2O_3	7.00	8.63	8.31	9.69	0.88	1.84	1.09	8.53	9.12	10.59
Ce_2O_3	27.55	29.49	28.84	32.86	5.61	15.78	7.97	28.72	25.23	19.44
Pr_2O_3	4.65	4.14	4.24	4.46	1.48	2.52	1.86	3.45	3.81	4.64
Nd_2O_3	19.35	18.17	17.92	17.50	12.00	14.61	13.60	14.07	16.45	18.63
Sm_2O_3	3.44	2.95	2.98	1.91	4.86	4.20	5.10	2.02	2.64	3.14
Eu_2O_3					0.24	0.14	0.22			
Gd_2O_3	1.61	1.40	1.47	0.91	4.46	3.22	3.90	0.96	0.92	1.35
Tb_2O_3					0.58	0.32	0.46			
Dy_2O_3	0.51	0.17	bd	bd	1.95	1.35	1.39	0.67	0.69	0.22
Er_2O_3					0.45	bd	0.34			
Yb_2O_3					0.33	0.21	0.30			
MgO	0.81	0.89	0.86	0.67		0.07	0.14			
CaO	4.40	3.93	4.33	3.54	11.42	5.61	10.08	6.29	6.92	7.08
MnO	0.07	0.07	0.13	0.10	0.10	0.14	0.15			
FeO*	1.33	1.31	1.43	2.31	4.59	4.28	4.13	0.32	0.16	0.37
SrO								1.21	1.20	1.49
BaO								bd	0.44	0.24
F	0.78	0.76	0.79	0.53	bd	0.22	0.22	0.81	0.95	0.91
Cl	0.08	0.07	0.07	bd						
Sum	95.58	95.41	95.22	97.00	83.60	84.84	85.14	71.93	72.47	71.66
O = F, Cl	0.35	0.34	0.35	0.22	0.00	0.09	0.09	0.34	0.40	0.38
Total	95.34	95.16	94.87	96.97	83.60	84.75	85.05	71.59	72.07	71.28
	Formulae on basis of 17 cations				*Formulae on basis of 2 Si*			*Formulae on basis of 1 cation*		
Ca	1.502	1.352	1.481	1.211	0.837	0.462	0.720	0.211	0.232	0.238
Sr								0.022	0.022	0.027
Ba								0.000	0.005	0.003
Th					0.002	0.015	0.002	0.009	0.010	0.008
La	0.822	1.022	0.979	1.141	0.022	0.052	0.027	0.098	0.105	0.123
Ce	3.213	3.468	3.371	3.841	0.140	0.444	0.194	0.329	0.289	0.223
Pr	0.540	0.484	0.493	0.519	0.037	0.071	0.045	0.039	0.043	0.053
Nd	2.201	2.084	2.043	1.995	0.293	0.401	0.324	0.157	0.184	0.209
Sm	0.378	0.326	0.328	0.210	0.114	0.111	0.117	0.022	0.028	0.034
Eu					0.006	0.004	0.005			
Gd	0.170	0.149	0.156	0.096	0.101	0.082	0.086	0.010	0.009	0.014
Tb					0.013	0.008	0.010			
Dy	0.052	0.018	0.000	0.000	0.043	0.033	0.030	0.007	0.007	0.002
Y	0.181	0.123	0.156	0.059	0.187	0.100	0.140	0.029	0.022	0.021
Fe^{2+}	0.354	0.352	0.382	0.617	0.262	0.275	0.230	0.008	0.004	0.010
Mn	0.019	0.019	0.035	0.027	0.006	0.009	0.008			
Al	0.120	0.125	0.079	0.026	0.000	0.035	0.000			
Mg	0.385	0.426	0.409	0.319		0.008	0.014			
Ti	0.055	0.048	0.062	0.065	0.006	0.006	0.004			
Si	6.844	6.859	6.866	6.800	2.000	2.000	2.000	0.058	0.039	0.035
P	0.154	0.136	0.154	0.057		0.032	0.000			
Be					2.000	2.000	2.000			
F	0.786	0.772	0.798	0.535	0.000	0.053	0.046	0.080	0.094	0.090
Cl	0.044	0.039	0.038	0.000						
Σ cations					6.07	6.20	6.00	1.000	1.000	1.000

Explanation: Analyses 1-2, intergrown with allanite-(Ce), Fig. 5b;3, 4, anhedral grains in chevkinite-(Ce); 5-7 agregate (Fig. 5b); X-Y, growing alongboundaries of allanite-(Ce). FeO* all Fe as Fe^{2+}. bd. below detection. Blank not determined. Be assumed to be 2.000 a.p.f.u.

Table 5. Representative compositions of cerite, hingganite and hydroxylbastnäsite-(Ce)

	1	2	3	4	5
wt.%					
P_2O_5	0.19	0.21	7.57	6.90	7.79
SiO_2	18.88	15.31	8.76	7.89	8.80
TiO_2	0.16	0.15	0.14	0.22	0.22
ThO_2	66.06	64.02	54.61	57.97	55.91
UO_2	3.89	0.99	0.62	0.50	0.55
Al_2O_3	bd	0.15	0.23	0.17	0.21
Y_2O_3	1.71	1.96	0.85	0.73	0.84
La_2O_3	0.13	0.32	2.00	1.61	1.80
Ce_2O_3	1.27	1.01	0.95	0.33	0.39
Pr_2O_3	bd	bd	0.74	0.36	0.33
Nd_2O_3	0.63	1.08	2.53	1.70	1.99
Sm_2O_3	0.27	0.60	0.55	0.29	0.40
Gd_2O_3	0.66	0.85	0.56	0.46	0.44
Dy_2O_3	0.55	0.44	bd	bd	bd
MgO	bd	0.05	0.08	0.06	0.06
CaO	0.03	1.02	2.76	3.07	2.50
MnO	bd	bd	0.08	bd	bd
FeO*	0.13	0.46	0.46	0.47	0.50
PbO	1.36	0.21	bd	bd	bd
Total	95.92	88.83	83.49	82.73	82.73
Formulae based on 4 oxygens					
P	0.009	0.011	0.380	0.362	0.392
Si	1.022	0.920	0.520	0.489	0.524
Ti	0.007	0.007	0.006	0.010	0.010
Th	0.814	0.876	0.737	0.818	0.757
U	0.047	0.013	0.008	0.007	0.007
Al	0.000	0.011	0.016	0.012	0.015
Y	0.049	0.063	0.027	0.024	0.027
La	0.003	0.007	0.044	0.037	0.040
Ce	0.025	0.022	0.021	0.007	0.008
Pr	0.000	0.000	0.016	0.008	0.007
Nd	0.012	0.023	0.054	0.038	0.042
Sm	0.005	0.012	0.011	0.006	0.008
Gd	0.012	0.017	0.011	0.009	0.009
Dy	0.010	0.009	0.000	0.000	0.000
Mg	0.000	0.004	0.007	0.006	0.005
Ca	0.002	0.066	0.175	0.204	0.159
Mn	0.000	0.000	0.004	0.000	0.000
Fe^{2+}	0.006	0.023	0.023	0.024	0.025
Pb	0.020	0.003	0.000	0.000	0.000
Σ cations	2.04	2.09	2.06	2.06	2.04

Explanation: Analyses 1, 2, anhedral grain in chevkinite-(Ce)(Fig. 5b); 3-5, string of grains in cerite -(Ce) (Fig. 5B). FeO* all Fe as Fe^{2+}. bd, below detection.

Table 6. Compositions of thorite